Evaluation of Observed Energy From Adiabatic Impact on Composite Lamenates

Dr. Kadhim H. Ghlaim*

Received on: 15/2/2009
Accepted on:5 /11/2009

Abstract

In this paper, the energy observed due to impact of conical projectiles on composite laminates is investigated. Four types of energies observed were studied. They are strain energy due to deformation of plate, large deformation near the impact zone, delaminating energy and energy losses due to friction.

The equation of motion of plate was developed for orthotropic laminated plate and solved with its boundary conditions. Large deformation of delaminated zone was derived assuming deformation shape formulation to calculate the penetration depth and delaminating radius. Delaminating energy was calculated by solving the delaminating failure criteria with equation of motion. Friction energy was calculated assuming constant friction coefficient.

The results show that the energy of deformation of plate is smaller than that for the large deformation and delaminating energy. And as cone angle increases the energy observed will be increased and the depth of penetration decreases. Numerical and experimental results quoted in published papers show a good agreement with that of the presented work.

Keywords: composites, delamination, impact, penetration.

تخمين الطاقة الممتصة نتيجة التصادم الاديباتي مع صفائح مركبة

الخلاصة

في هذا البحث تم التخمين النظري للطاقة الممتصة نتيجة اختراق اطلاقة جاسئة مخروطية لصفيحة طباقية مركبة, تم تقسم الطاقات الممتصة الى اربعة انواع, هي طاقة الانفعال نتيجة تشويه الصفيحة, طاقة التشويه العالي حول منطقة الاصطدام, طاقة التفصخ و الطاقة الممتصة نتيجة الاحتكاك.اشتقت معادلة الحركة المطورة للصفيحة الطباقية المركبة وحلت بمعلومية الشروط الحدية لها. كذلك تم معالجة منطقة التشويه العالي بطريقة مبتكرة هي طرية افتراض شكل التشويه ومن حلاله تم تخمين قطر منطقة التفصخ. ومن ثم تم احتساب طاقة التفصخ باستخدام معامل التفصخ المعتمد وتعويضه في معادلة الحركة المطورة. بينما تم احتساب الطاقة الممتصة خلال الاحتكاك تحت فرضية ثبوت معامل الاحتكاك.

اظهرت النتائج ان طاقة الانفعال الممتصةهي اقل من طاقة التشويه العالي و كذلك اقل من طاقة التفصخ. وكذلك اظهر النتائج زيادة في الطاقة الممتصة ونقصان في عمق الاختراق عند نقصان زاوية مخروط الاطلاقة. تم مقرنة النتائج مع اعمال عددية و عملية منشورة وانتجت توافقا مقبولا اثبت اهلية الحل النظري المقترح مع امكانية تطوير اكثر مستقبلا.

* **Dijlah University College /Baghdad**

https://doi.org/10.30684/etj.28.8.5
2412-0758/University of Technology-Iraq, Baghdad, Iraq

List of symbols

A	Area	m^2
a	Delamination	m
a	Width of	m
b	Length of	m
E	Young	MPa
F	Friction force	N
G	Modulus of	MPa
h	Plate	m
J	Area moment	m^4
q	Impact force	N
R	Deformation	M
t	Time	s
u	Displacement	m
U	Energy	J
V	Velocity	m/s
x	Direction	m
y	Direction	m
z	Direction	m
α	Shear	-
β	Angle	rad
ε	Longitudinal	-
ϕ	Projectile	rad
γ	Shear strain	rad
κ	Curvature	m^{-1}
μ	Friction	-
ν	Poisson's	-
θ	Slope	rad
ρ	Density	kg/m3
σ	Longitudinal	MPa
τ	Shear stress	MPa

Introduction

To analyze the impact response problems, it is obvious that an accurate account of the contact behavior is one of the most important steps. The classical contact law between elastic spheres and an elastic half-space derived by Hertz[1] has been used by many authors for studying impact response of homogenous isotropic materials [2]. In studying impact response of laminated composites, however the problem becomes more complicated [3].

One may easily realize that Hertzian contact law, which was based on assuming a homogenous isotropic materials, may not be

adequate in describing the contact behavior on laminated composite due to their anisotropic and non-homogenous properties.

Moreover, most of the limited composites used are quite thin and cannot be represented by

half-space in the existing analytical work[3-5], leading of limits were assumed known, and the responses of the laminates assumed elastic.

Tan and Sun [4] and Guan and Yang [5] gave the development history of the contact problem through the low velocity impact. These models with their developments were used by authors to evaluate the response and compared it with experimental results.

Although some of the high and ballistic velocity impact damage mechanics are similar to those at low velocity, the response of a structure composite is different and more complex. Furthermore, it is also more difficult to test at high and ballistic velocities.

Since the contact time between the projectile and the composite is considerably less at ballistic velocities, the impact loading induced localized response with no global deformation. This concept was demonstrated by looking at delamination in beams of various lengths impacted at low and high velocities [6,7]. It was found that the damage size decreases with increasing the length of beam for low velocity impact. At high velocity, however, the level of damage was independent of the length of beam.

Since the high velocity impact energy is dissipated over a smaller region, an additional damage mechanism is presented at high velocities known as the shear plug. Due to the stresses created at the point of impact, the material around the perimeter of the projectile is sheared and pushed foreword causing a hole or "plug", slightly larger than the diameter of the projectile[7].

The fiber properties have the major effect for absorbing energy due to high velocity impact, the experimental results indicated that the rate of energy absorption of the panel increases drastically with the fiber modulus, but the very high modulus material tends to exhibit poor impact resistance due to its low working strain. Aramid fiber seems to exhibit the best combination of high modulus while steel maintaining reasonable high breaking strain [8]. While the absorbed energy was found to be a linear relation with the thickness of the composite laminate insuring that the weight efficiency of the fiber composite is greater than the metallic target like steel[9]. For this important effect of the fiber mechanical properties, and the fabrication of hybrid composites from multi types of layered fibers was used [9]. The technique of interlaminate hybridization was found to enhance delamination under impact loading. Delamination was found to be an effective energy absorbing in hybrids. The impact energy absorption capability depends on which side face the impact direction. In general, the unsymmetric hybrids have better impact properties than

their alternating sequence counterparts. In most cases, failure in these materials involved perforation, delamination and some tearing of the more brittle layers in conjunction with deflection of the tougher layers, provided the tougher side faced the impact direction. When the more rigid side was struck first, this stiff layer was perforated with a lesser degree of plastic deformation.

When the kinetic energy of impactor is greater than ballistic range, the perforation takes place. Now the ballistic limit of velocity will be the additional parameters added to the parameters study in the high velocity impact. Ballistic velocity is the impact velocity that gives the ability for full penetration without remaining energy. The energy required achieving target perforation and ballistic limit remaining invariant of specimen geometry [10,11]. To avoid the perforation especially for the designing of personal body armor, aramid or spectra fiber composite was used, for this application the repeated impact was used to know the striking velocity[10]. The ballistic limit was increased with Areal density[12,13] and the striking velocity decreased with the number of repeated impact, while the delamination zone was increased.

3. Theory

Based on the conservation of the total energy, the part of the kinetic energy of the projectile is absorbed by the plate, and assumed to be classified into four types which are: -

1- The strain energy due to dynamics of plate's theory (Contact energy) U_c .
2- Strain energy in the large deflection penetration zone U_{Ld} .
3- Delamination strain energy U_{del}.
4- Friction energy U_F.

The energy balance according to this classification for the impact becomes

$$\frac{1}{2} M_p V_{pi}^2 = + U_c + U_{Ld} + U_{del} + U_F + \frac{1}{2} M_p V_{po}^2 \quad \dots (1)$$

Strain energy due to deformation of plate

The equation of motion for the laminated composite plate subjected to dynamic load (impact) is [14]

$$D_{11}\frac{\partial^4 w}{\partial x^4}+4D_{16}\frac{\partial^4 w}{\partial x^3 \partial y}+2(D_{12}+D_{66})\frac{\partial^4 w}{\partial x^2 \partial y^2} \quad \dots(2)$$
$$+4D_{26}\frac{\partial^4 w}{\partial x \partial y^3}+D_{22}\frac{\partial^4 w}{\partial y^4}+rh\frac{\partial^2 w}{\partial t^2}=q$$

w(x,y) is the deflection along the z direction. q(x,y,t) is the intensity of transverse distributed load per unit area acting on the thin plate.D_{11}, D_{16}, D_{12}, D_{66}, D_{26}, D_{22} are the flexural rigidity coefficients of the laminated plate.

For especially orthotropic laminates (D_{16} = D_{26} =0), the governing differential equation becomes.

$$D_{11}\frac{\partial^4 w}{\partial x^4}+2(D_{12}+D_{66})\frac{\partial^4 w}{\partial x^2 \partial y^2}+D_{22}\frac{\partial^4 w}{\partial y^4}+\rho h\frac{\partial^2 w}{\partial t^2}=q(x,y,t) \quad \dots(3)$$

The force for this plate is dynamics impact force, which is obtained from the modified Hertzian contact theory.

Contact Law

The relationship between the impact force P and contact deformation α is given by Hertz Contact Law[5]

$$q = nw_m^{1.5} \quad \ldots(4)$$

where the contact deformation is the distance between the center of the projectile's nose and the mid-surface of the beam and n is the modified constant of the Hertz Contact Law proposed by Tan and Sun[4].

$$n = \frac{4}{3}\sqrt{R_p}\,\frac{1}{\left[(1-\nu_p)/E_p + 1/E_{c22}\right]} \quad \ldots(5)$$

where R_p, ν_p , E_p are the local radius, Poisson's ratio, and Young's modulus of the projectile, respectively. E_{c22} is the transverse modulus normal to the fiber direction in the surface ply facing the projectile.

The solution of the dynamic of plate equation (3) is by using the finite difference method, the Details of the solution is derived through the Ph.D work by Ali Al Hilli [16], this solution was required for the equivalent elastic wave speed and the natural frequency to optimize the best time and distance increments, the details of finding the natural frequency for rectangular clamped plates (CCCC plates) is shown [14].

The strain energy for these cases was evaluated numerically from the integration of strain energy through the plate area using[14]

$$U_\epsilon = \int_0^b \int_0^a \left[D_{11}\left(\frac{\partial^2 w}{\partial x^2}\right)^2 + 2D_{12}\frac{\partial^2 w}{\partial x^2}\frac{\partial^2 w}{\partial y^2} + D_{22}\left(\frac{\partial^2 w}{\partial y^2}\right)^2 + D_{66}\left(\frac{\partial^2 w}{\partial x \partial y}\right)^2 \right] dxdy \quad \ldots(6)$$

Strain energy due to deformation of delamination zone, (assumed deformation shape formulation)

Assumptions

i- Delamination occurs at all layers.

ii-The delaminations areas are approximately circular and this area covers the large deformation zone.

Consider the large deformation circular zone shown in Fig 1.

For layer i

$$\frac{y_i}{r_i} = \frac{y}{d/2} \quad \ldots(7)$$

r_i: hole radius of layer i through penetration

y_i : height of cone penetrate the layer i

R_i: radius of curvature of layers i in the delamination zone, which is assumed to be constant.

$$r_i = a - R_i\, sin(\phi/2) \qquad \text{Then}$$

$$R_i = \frac{a - r_i}{sin(\phi/2)}$$

$\phi/2$: half cone angle of the impactor.

Consider a washer element in the ply i (deformed ply) has a radius r then

$$r = a - R_i\, sin(\theta)$$

Using the volume constancy of the delamination area after and before the penetration, then

$$\pi a^2 h = \int_0^{\phi/2} 2\pi r h R_i\, d\theta$$

$$a^2 = 2\left(\frac{a - r_i}{sin(\phi/2)}\right)\left(\frac{a\phi}{2} + \frac{a - r_i}{tan(\phi/2)}\right)$$

Multiply by $\sin^2(\phi/2)$ and rearrange the equation

$$a = \frac{c_1 \pm c_2}{c_3} \quad \ldots(8)$$

$$c_1 = -2r_i f - 4r_i \cot(f/2)$$

$$c_2 = \left[\{r_i f + 4r_i \cot(f/2)\}^2 - 4\{\sin(f/2) - f - 2\cot(f/2)\} \times 2r_i \cot(f/2)\right]1/2$$

$$c_3 = 2[\sin(f/2) - f - 2\cot(f/2)]$$

The equation (8) has two unknowns which are the delamination radius "a" and the hole radius of the ply "r_i", then a second equation is needed to calculate the unknowns which is the failure criteria of the delamination zone.

Energy observed due to delamination itself

The failure criterion for delamination is given by[5]: -

$$F_{delam} = \left(\frac{\sigma_n}{S_n}\right)^2 + \left(\frac{\sigma_s}{S_s}\right)^2 \quad \ldots(9)$$

Where σ_n and σ_s are the normal and shear interface stresses, respectively, and S_n and S_s are the corresponding strength, delamination occurs when $F_{delam} \geq 1$.

From curvature of plate shown in Fig. 1.

$$R_i = \frac{a - r_i}{sin(\phi/2)}$$

The strain can be calculated using $\kappa_\theta = \frac{1}{R_i}$.

For Cartesian coordinates,

$$x = r\,cos(\beta) \qquad r = \sqrt{x^2 + y^2}$$

$$y = r\,sin(\beta) \qquad \beta = tan^{-1}\frac{y}{x}$$

Now that $\kappa_x = \frac{-\partial^2 w}{\partial x^2}$, $\kappa_y = \frac{-\partial^2 w}{\partial y^2}$, $and\ \kappa_{xy} = \frac{-\partial^2 w}{\partial x \partial y}$

And in polar coordinates $\kappa_r = \frac{-\partial^2 w}{\partial r^2}$, $and\ \kappa_\theta = -\frac{1}{r^2}\frac{\partial^2 w}{\partial \theta^2}$

From geometry

$$w = R_i(1 - cos(\theta))$$

$$r = a - R_i\,sin(\theta)$$

I.e. $R_i = \left(\frac{a-r}{sin(\theta)}\right)$ and

$$\theta = sin^{-1}\left(\frac{a-r}{R_i}\right)$$

$$dr = -R_i\,cos(\theta)\,d\theta$$

$\frac{\partial w}{\partial r} = \frac{(1 - cos(\theta))}{sin(\theta)}$, then $\frac{\partial^2 w}{\partial r^2} = 0$ and

$$\frac{\partial w}{\partial \theta} = (a-r)\left(csc(\theta)\,cot(\theta) + csc^2(\theta)\right)$$

$$\frac{\partial^2 w}{\partial \theta^2} = (a-r)\left(sec^3(\theta) + esc(\theta)\,tan^2(\theta) - 2csc^3(\theta)\,cot(\theta)\right)$$

Using step by step chain rule $\frac{\partial w}{\partial x} = \frac{\partial w}{\partial \theta}.\frac{\partial \theta}{\partial x}$ And $\frac{\partial w}{\partial y} = \frac{\partial w}{\partial \theta}.\frac{\partial \theta}{\partial y}$ &

$$\frac{\partial \theta}{\partial x} = \frac{-2x(1/2)}{\sqrt{x^2+y^2}\,R_i\sqrt{1 - \left(\frac{\sqrt{x^2+y^2}}{R_i}\right)^2}}$$

$$\frac{\partial q}{\partial y} = \frac{-2y(1/2)}{\sqrt{x^2+y^2}\,R_i\sqrt{1 - \left(\frac{\sqrt{x^2+y^2}}{R_i}\right)^2}}$$ This

gives

$$\frac{\partial \theta}{\partial x} = \frac{-x}{r\sqrt{R_i^2 - r^2}} \text{ and } \frac{\partial \theta}{\partial y} = \frac{-y}{r\sqrt{R_i^2 - r^2}}$$

Then

$$\frac{\partial w}{\partial x} = \frac{-x}{r\sqrt{R_i^2 - r^2}}(a-r)\left(csc(\theta)\,cot(\theta) + csc^2(\theta)\right)$$

And

$$\frac{\partial w}{\partial y} = \frac{-y}{r\sqrt{R_i^2 - r^2}}(a-r)\left(csc(\theta)\,cot(\theta) + csc^2(\theta)\right)$$

$$\frac{\partial^2 w}{\partial x^2}=\frac{\partial}{\partial\theta}\left(\frac{\partial w}{\partial x}\right).\frac{\partial\theta}{\partial x}\text{ and}$$

$$\frac{\partial^2 w}{\partial y^2}=\frac{\partial}{\partial\theta}\left(\frac{\partial w}{\partial y}\right).\frac{\partial\theta}{\partial y}$$

$$\frac{\partial^2 w}{\partial x^2}=\frac{x^2}{r^2\left(R_i^2-r^2\right)^2}(a-r)\left(csc(\theta)\,cot(\theta)+csc^2(\theta)\right)=-\kappa_x$$

$$\frac{\partial^2 w}{\partial y^2}=\frac{y^2}{r^2\left(R_i^2-r^2\right)^2}(a-r)\left(csc(\theta)\,cot(\theta)+csc^2(\theta)\right)=-\kappa_y$$

$$\frac{\partial^2 w}{\partial x\partial y}=\frac{\partial}{\partial\theta}\left(\frac{\partial w}{\partial x}\right).\frac{\partial\theta}{\partial y}$$

$$\frac{\partial^2 w}{\partial x\partial y}=\frac{xy}{r^2\left(R_i^2-r^2\right)^2}(a-r)\left(csc(\theta)\,cot(\theta)+csc^2(\theta)\right)=-\kappa_{xy}$$

From plate bending theory

$$\begin{Bmatrix}\varepsilon_x\\ \varepsilon_y\\ \gamma_{xy}\end{Bmatrix}=\begin{Bmatrix}\varepsilon_x^o\\ \varepsilon_y^o\\ \gamma_{xy}^o\end{Bmatrix}+z\begin{Bmatrix}\kappa_x\\ \kappa_y\\ \frac{1}{2}\kappa_{xy}\end{Bmatrix}$$

With assumption of zero mid-span strain

$$\begin{Bmatrix}\varepsilon_x\\ \varepsilon_y\\ \gamma_{xy}\end{Bmatrix}=z\begin{Bmatrix}\kappa_x\\ \kappa_y\\ \frac{1}{2}\kappa_{xy}\end{Bmatrix}$$

$$=\frac{-z(a-r)\left(csc(\theta)\,cot(\theta)+csc^2(\theta)\right)}{r^2\left(R_i^2-r^2\right)^2}\begin{Bmatrix}x^2\\ y^2\\ \frac{1}{2}xy\end{Bmatrix}$$

For ply $\begin{Bmatrix}\sigma_x\\ \sigma_y\\ \sigma_{xy}\end{Bmatrix}=[\overline{Q}]\begin{Bmatrix}\varepsilon_x\\ \varepsilon_y\\ \varepsilon_{xy}\end{Bmatrix}$

For interface and assuming plane strain problems

$$\begin{Bmatrix}\sigma_x\\ \sigma_y\\ \tau_{xy}\end{Bmatrix}=[D]\begin{Bmatrix}\varepsilon_x\\ \varepsilon_y\\ \gamma_{xy}\end{Bmatrix}\qquad\ldots(10)$$

Where

$$[D]=\frac{E_m(1-\nu_m)}{(1+\nu_m)(1-2\nu_m)}\begin{bmatrix}1 & \frac{\nu_m}{1-\nu_m} & 0\\ \frac{\nu_m}{1-\nu_m} & 1 & 0\\ 0 & 0 & \frac{1-2\nu_m}{2(1-\nu_m)}\end{bmatrix}\qquad(11)$$

ν_m and E_m are Poisson's ratio and elasticity modulus of matrix respectively. Substitute equation (11) in equation (10) and rearrange, it gives

$$\begin{Bmatrix}\sigma_x\\ \sigma_y\\ \tau_{xy}\end{Bmatrix}=\frac{E_m(1-\nu_m)}{(1+\nu_m)(1-2\nu_m)}\left\{\frac{-z(a-r)\left(csc(\theta)\,cot(\theta)+csc^2(\theta)\right)}{r^2\left(R_i^2-r^2\right)^2}\right\}\begin{bmatrix}1 & \frac{\nu_m}{1-\nu_m} & 0\\ \frac{\nu_m}{1-\nu_m} & 1 & 0\\ 0 & 0 & \frac{1-2\nu_m}{2(1-\nu_m)}\end{bmatrix}\begin{Bmatrix}x^2\\ y^2\\ \frac{1}{2}xy\end{Bmatrix}$$

…(12)

From maximum principal stress and shear stress

$$\sigma=\frac{\sigma_x+\sigma_y}{2}+\sqrt{\left(\frac{\sigma_x-\sigma_y}{2}\right)^2+\tau_{xy}^2}\qquad\text{and}$$

$$\tau=\sqrt{\left(\frac{\sigma_x-\sigma_y}{2}\right)^2+\tau_{xy}^2}$$

Substitute in equation (9), it yields another equation containing radius r_i and delamination radius a. Solve with equation (8) to get the delamination ***a*** and the hole radius of ply i due to penetration. The same steps can be repeated for all penetrated plies.

The strain energy for the deformation of large deformation zone is

$$U_{Ld}=4\sum_{i=1}^{n}\int_0^{\pi/2}\int_0^{r_i}\left[D_{11}\left(\frac{\partial^2 w}{\partial x^2}\right)^2+2D_{12}\frac{\partial^2 w}{\partial x^2}\frac{\partial^2 w}{\partial y^2}+D_{22}\left(\frac{\partial^2 w}{\partial y^2}\right)^2+D_{66}\left(\frac{\partial^2 w}{\partial x\partial y}\right)^2\right]r\,dr\,d\theta$$

…(13)

While the delamination energy is

$$U_{del}=\pi D\sum_{i=1}^{n}\int_0^{a}\left(\frac{\partial^2 w}{\partial r^2}+\frac{1}{r}\frac{\partial w}{\partial r}\right)^2 r\,dr\ldots(14)$$

Friction energy

This observed energy is required to calculate the friction coefficient between the impactor and

the plies. The friction process is very difficult due to delamination, change in area of the contact, and load with time and thermal effect on the friction. Also after delamination there are other losses in energies due to friction in delamination of plies.

The friction coefficients between the composite and the projectile material are measured using friction disk with the details shown in the next chapter.

The assumptions used in the friction work are that the friction is independent on the heat generation through the penetration. This

Using the momentum equation for the projectile

$$m(Vi-Vr)=\int_0^{tp}(q-F\cos(\phi/2)-\mu F\sin(\phi/2)dt \quad \ldots(15)$$

The energy absorbed for friction is

$$U_F = \int_0^{h/\cos(\phi/2)} Fds \quad \ldots(16)$$

4.Results and Discussions

The theoretical model developed in this work using the conservation of energy is divide the absorbed energy into four branches which are elastic-dynamic deformation of plate, contact energy, strain energy of the penetration zone, delamination energy and friction energy. The details of the results for every type of these energies are presented.

The composite materials used in this work have the mechanical properties listed in Table 1. The plates which are studied for the theoretical model has 80*80 mm^2 in area and the thicknesses are the remaining parameters studied throughout the work. The equation of assumption is fair especially because the penetration time is very small to transfer heat through the surfaces. The Friction due to delamination is small with low movement compared with the friction due to penetration which vary clear in the geometry of the penetration and friction, and because the delamination energy was considered, then the friction through the delamination was considered through the analyses of the delamination [figure 2] . Then the analyses of frictional energy is based on the variation of penetration loads through the penetration.

motion for the composite plates requires the impact excitation force. So the modified contact Law was used. Fig.3 shows the contact force verses the middle deflection of the plate. The contact law was independent of the thickness of the plate; therefore the figure contained the curves for composite used without reference to the thickness. Then this represents the contact stiffnesses for these materials. It has been shown that the contact stiffness is higher for the high modulus materials such as Kevlar composite. And because the modulus for the resting materials was in the same order then the contact stiffnesses for these materials were closely related together.

The first mode natural frequency of the plate is determined for the materials studied for different thicknesses as shown in Fig.4. Use of the first mode of fragments natural in the impact analysis is due to large deflection that occurs through the impact. The natural frequency increases with increasing the thickness and this gives the ability to

use longer increment time for the finite difference simulation. It was shown that the natural frequency increased with increasing the modulus of elasticity because the stiffness for higher modulus material was higher.

The equivalent elastic wave speed for the composite materials is shown in Fig.5. The elastic wave speed in proportional to the modulus of elasticity and inversely proportional to the density of the material, because of that it is shown that the Kevlar composite has higher wave speed then the other composites

From the elastic wave speed and the natural frequency of studied the materials the time increment for the finite difference solution of the dynamic equation was estimated using the domain and the details are given in appendix A. Through the solution of the (Matlab 6.5) program built for this purpose the time and displacement increment was calculated. The program gave the ability to draw the deflection that occurs at the end of the period of the elastic dynamic deformation which occurred when the maximum stresses calculated through the running of the program (through the contact force that penetrates the plate elastically) reaching the ultimate stress for the front layer for the composite plate.

The results of the maximum force for different thicknesses of plate ranged from 1 to 10 mm and for different incident velocities ranged from 50 to 600 m/s for the materials are shown in Figures 6 to Figures 13 for different composite mateials.

The figures are plotted in the three dimensional forms where the vertical axis represents the maximum contact force before the failure penetration takes place, the left axis represents the variation in thickness and the right axis represents the variation in the incident velocity. It has been shown that the Kevlar composite carried the maximum value of maximum force due to impact as shown the largest value for q in its Fig. 13. The maximum force to be carried by the composite for the elastic impact zone increased with increasing the plate thickness because the resistance to the deformation due to contact is increased with the thickness, which was called, the stiffness.

It has been shown that the contact force increased with increasing the velocity of the projectile; this is because increasing the velocity means increasing its momentum. Consequently the of force and momentum the latter will increases.

Figure 14 shows the deformation shape of clamped two layers 3-end satin fiber reinforced polyester plate (80*80mm) impacted by 7.5g rigid impactor with V_i=100m/s and r_p=1mm. This ensures that the first mode natural frequency is in agreement with the choice of the optimally when the increment time for the finite difference and for showing the deformation shape occurs for the plate in the elastic zone. It has been shown that the shape of the deformation is equivalent to the first mode shape for frequency of

clamped composite plate [15]. The maximum deflection is located in the middle of the contact point with the impactor. And the special orthotropity for the woven style for the fiber is affected for the symmetry of the deformation through the two principal dimensions of the plate. The other phenomena can be shown is the polar symmetry that occurs near the contact point. This gives the reason and fixation of the presented assumption that the delamination area is circular for the woven composite plate subjected to lateral impact force.

The contact energy absorbed through the impact of the contact force shown previously is shown in figures (15- 22) for the materials studied.

From all these results it has been shown that the Kevlar composite has higher contact energy absorbed because it carries a higher value for contact force as discussed earlier. The carbon fiber composite is the second for absorbing contact energy; the E-Glass composite was the third. The arrangement is the same for these materials for the mechanical properties as discussed earlier.

The contact energy and contact force are in the order for the E-Glass and Carbon Composites while the Kevlar composite has higher values for contact energy and force. The contact force and energy increased with increasing incident velocity because of increasing momentum. And increased with increasing thickness of the composite plate due to the increase of the stiffness.

The remaining absorbing energy were solved together because those energies give the final results for the impact. For example the number of layered delaminated which is entering on the delamination energy should be investigated. Other type of absorbing energies is the penetration for large deformation energy, which must be solved with the delamination energy to calculate the delamination area and penetration radius. And previous type must be solved with the friction losses to estimate the final shape after impact and the type of penetration (partial or fully penetration). The results below for the energies are coupled together to give these results. The delamination energy for the materials used gives the delamination radius as a side result for this analysis. The delamination radius versus local projectile radius is shown in Fig.27 for different projectile cone angle.

It has been shown that the delamination radius is increased with increasing penetration radius and half cone angle of the projectile. As the projectile penetrates the ply, the local penetration radius will be increased and this gives to increasing the large deformation zone and then the delamination radius will be increased. The cone angle of the projectile has an affect on the penetration hole positively and because of that it depends directly on the delamination radius The comparisons of the contact force and energy for different materials with constant thickness (4mm) and with constant incident velocity (250m/s) are shown in Fig.23 and Fig.24 respectively for contact force. And

for the energy is shown in Fig.25 and Fig.26.

The types of absorbing energies for the plate are shown in Fig. 28 for material Plain-woven 2.5*2.5 E-Glass reinforced polyester for 4mm thickness. It has been shown that the contact elastic energy is negligibly small compared with the other types of absorbing energies.

The delamination and large deformation energy increased as the impact velocity increased until reaching the fully penetration zone after that the delamination and large deformation energy stay constant for all velocities upper the velocity for just penetration. This velocity was called the ballistic limit velocity for the plate.

Before the full penetration the velocity increases the penetration depth will be increased causing an increase in the delamination area and large deformation zone, which cause increasing the delamination and large deformation energies. It has been shown that the friction energy continuously increased as the velocity of impact increases, this is because of increase in the momentum of the impact and so the impact force will increases causing an increase in the friction energy.

The kinetic energy and absorbed energy verses incident velocity for 10 layers (4m thickness) is shown in Fig.29. It has been shown that the absorbed energy increased as the incident velocity increases in a rate smaller than the rate on increasing kinetic energy. The kinetic energy was increased with the square power of the incident velocity while the absorbed energy increases as the momentum increases and the friction force increases. It will be noticed that the absorbed energy depends on the incident vel to cheek the model an impact tests were carried out. The impact tests are done for the fabricated specimens will be tested. For this reason the 10-layers plain woven E-Glass reinforce polyester composite plate 4mm thickness and 100*100 mm squared. The clamping reduces the dimensions to 80*80mm. The results for these tests are shown in Fig. 30. The material used in the tests is the same as that shown in the analytical solution shown in Fig. 29. A fare agreement was presented for the velocity near the ballistic limits and the experimental amount of the absorbed energy will be greater than that for the analytical solution because excess amount of energy absorbed due to matrix cracks and fragmentation which are not included in the present model. The results of the test shown in Fig. 30 shows that the resting velocity increased as the incident velocity increases because the resting energy is not absorbed and increases with the incident velocity. The penetration time measured decreased as the incident velocity increases due to high velocity with constant thickness giving the shortest time. The absorbed energy increases as the incident velocity increases due to increase in the deflection, delamination and fragmentation. These results are similar to the analytical results.

5. Coclusions

The new analytical model for impact mechanics of conical prjectile on composite materials was derived. This analytical model is based on the energy balance through the impact. Through this balance four types of energies are assumed to be absorbed through the impact, these are contact energy, delamination energy, large deformation energy absorbed near the contact zone and friction energy.

The main conclusions of that can be drawn are:

1. The carbon fibers reinforced composites have a higher energy absorbed due to impact than that of the E-Glass reinforced composites and lower than that of the Kevlar reinforced composites.
2. The contact force and energy increases as the thickness of the plate increases, and both the mechanical properties and the incident velocity increase.
3. The wave speed increased as the Young's modulus increases, then the Carbon fibers composites have higher wave speeds than that of E-Glass composites and lower than that of Kevlar composites.
4. The delamination area increases as the cone angle of projectile increases and the radius of projectile increases.
5. In general, as the incident velocity increases the energy absorbed due to impact increases.
6. The contact energy is found to be negligibly small and its effect decreased as the incident velocity increases.
7. The delamination and large deformation energies are found to be increased as the incident velocity increases near the ballistic limit velocity and when the incident velocity increases above these limits the two energies are kept constant.
8. The friction energy has small effect for the velocity range lower the ballistic limits and its effect was increased as the velocity increased above the ballistic limit until it has the main effect for the total absorbing energy.
9. The absorbing energy due to impact is found to be higher for composite materials that have the higher mechanical properties.

6.Referances

[1] Greszczuk L. B.," Response of Isotropic and Composite Materials to Particle Impact", Foreign Object Impact Damage to Composite, ASTM STP 568, American Society for Testing and Materials, pp 183-208, (1975).

[2] Jonsan A. Zakus, T. Nicholas, H. F. Swift, L. B. Greszczuk, Curran D.R.," Impact Dynamics", John Wiley and Sons, Inc. (1982).

[3] Enboa Wu and Ching-Shih Yen," The Contact Behavior Between Laminate Composite Plate and Rigid Spheres" Trans. ASME (Journal of Applied Mechanics), Vol.6, PP 60-67, (1994).

[4] Tan and Sun," Used of Static Indentation Laws in the Impact Analysis of Composite Plates", Trans. ASME, Vol.52, pp.6-12, (1985).

[5] Zhidong Guan and Chidar Yang," Low Velocity Impact Damage Process of Composite Laminate", Department of Mechanical Engineering, Wichita state University, (2000).

[6] De Moura M.F.S.F and Goncalves J.P.M., " Modeling the Interaction Between Matrix Cracking and Delamination in Carbon-Epoxy Laminates Under Low Velocity Impact", Composites Science and Technology, Vol.14, pp.1021-1027, (2004).

[7] Roger Ellis L.," Ballistic Impact Resistance of Graphite Epoxy Composites With Shape Memory Alloy and Extended Chain Polyethylene Spectra Hybrid Components" MSc. Thesis, Virginia Polytechnolic Institute and State University, (1996).

[8] David Raylance," Influence of Fiber Properties on Ballistic Penetration of Textile Panels", Composite Science and Technology, Vol.14, pp.183-190,(1981)

[9] Gupta B. P. and Davids N.," Penetration Experiments with Fiberglass-Reinforced Plastic", Experimental Mechanics, pp.445-450, (1966).

[10] Canwell W.J. and Morton J.," Impact Perforation of Carbon Fiber Reinforced Plastic", Composite Science and Technology, Vol.38, pp.119-141, (1990).

[11] Dutta P.K., Farrell D., Taylor S., Aziz Tadayon and David Hui. ," Ballistic Perforation of Graphite/Epoxy Composite", (Special Report 96-29), US Army Corps of Engineers, December (1996).

[12] Lee B.L., Song J.W. and Ward J.E.," Failure of Spectra Polyethylene Fiber-Reinforced Composites under Ballistic Impact Loading", Journal of Composite Materials, Vol.28, No.3, pp.1202-1226, (1994).

[13] Frank K.Ko, Amotz J.G. and Song W.S.," Behavior of Gradient Designed Composite Under Ballistic Impact", Proceeding of ICCM-11, Gold Coast, Australia, Vol. II, pp.414-473,4th-18th July (1997).

[14] Rao J.S.," Dynamics of Plate", Narosa Publishing House, 1999.

[15] Bohe Wang," The Application of Finite Difference Method and Matlab in Engineering Plates", M.Sc. thesis, West Virginia University, 1999.

[16] Ali Hussain Al Hilli, " Analytical and Experimental Analysis of High Velocity Impact on Composite Plate Targets", Ph.D thesis, Nahrain University 2006.

Table (1) The measured mechanical properties for the composites manufactured

Composition		Woven composite ply				
Fiber	Matrix	Style	s_{ult}	$E_1=E_2$	n	G_{12}
E-Glass	Epoxy	Plain (2.5*2.5)	53.94	2611	0.096	473
E-Glass	Polyester	Plain (2.5*2.5)	46.61	2226	0.112	474
E-Glass	Polyester	Plain (12.5*12.5)	43.45	2051	0.093	448
E-Glass	Polyester	5-end satin (5*5)	41.08	2138	0.045	455
E-Glass	Polyester	Random	32.39	3184	0.231	1293
Carbon	Polyester	Plain (7*7)	54.6	3023	0.061	583
Carbon	Polyester	5-end satin (5*5)	59.85	3512	0.085	550
Kevlar	Polyester	3-end satin (7*7)	166.8	9517	0.043	852

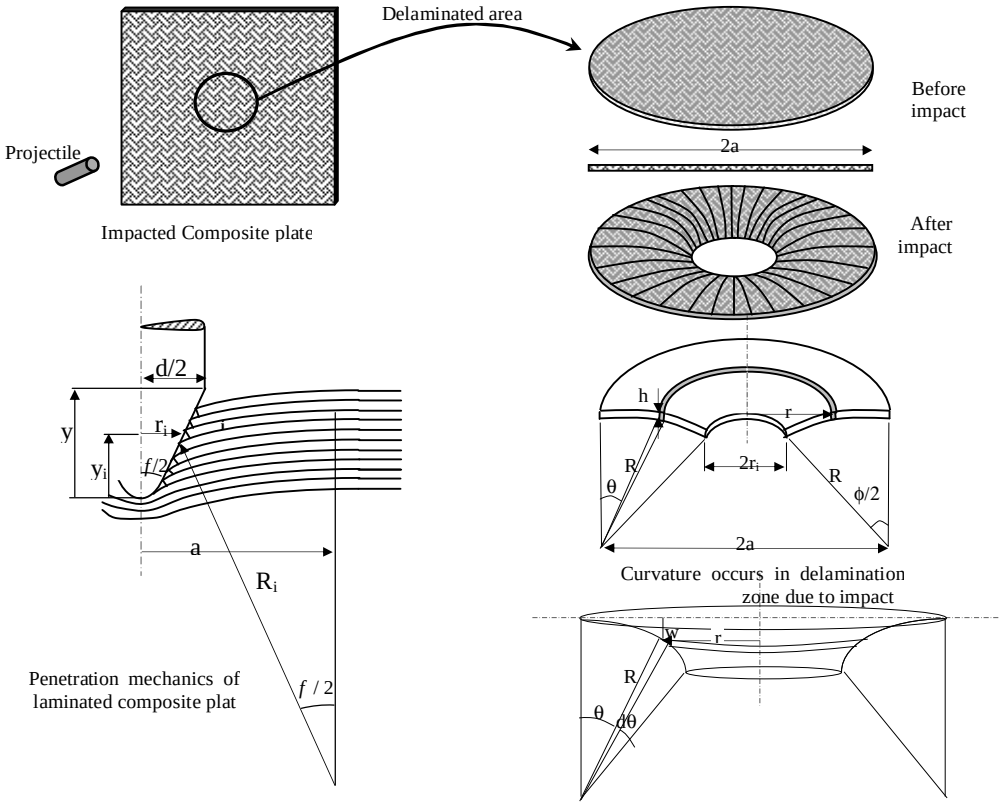

Figure (1) Schematic drawing represent the impact delaminated large deformation and penetration zone.

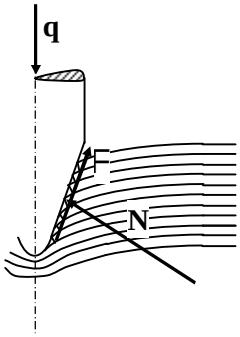

Figure (2) the normal force and friction through the impact penetration load

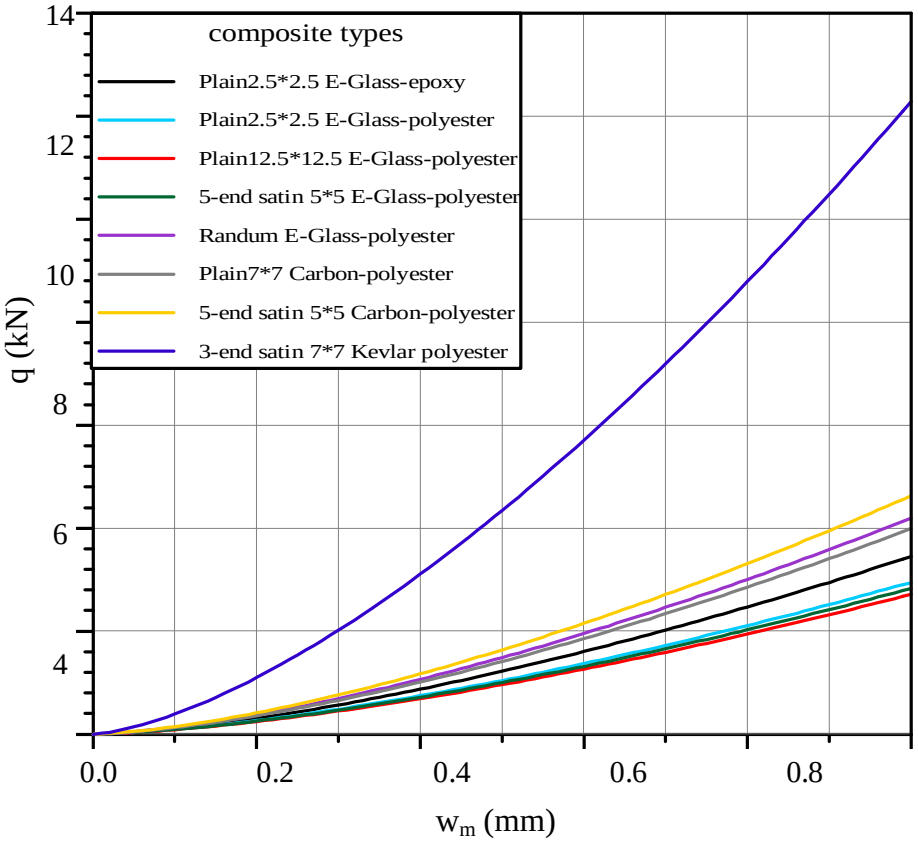

Figure (3) Contact force q verses plate meddle deflection (w_m) for the composite used

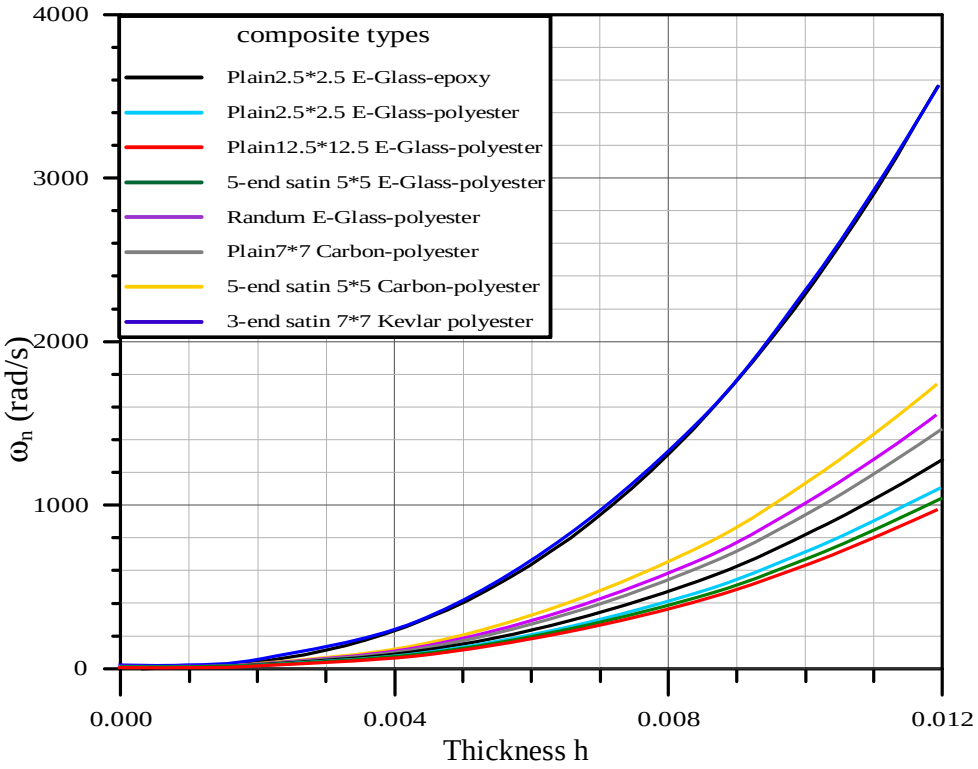

Figure (4) Natural frequency verses thickness of plates for the composite materials used

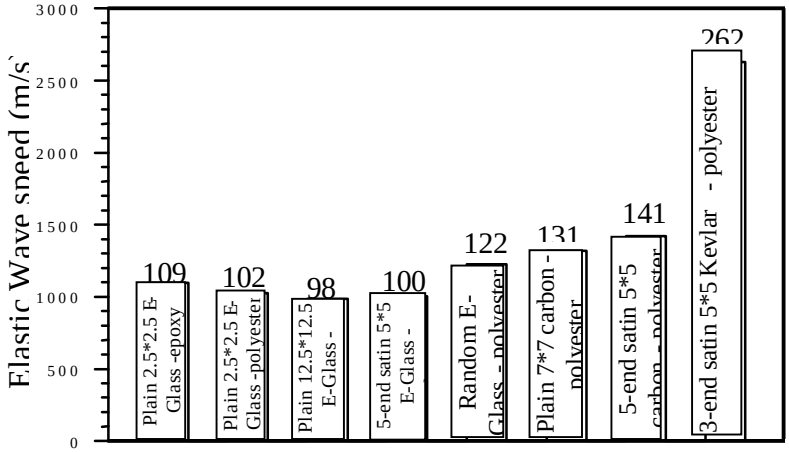

Figure (5) Approximate Elastic wave speed for the composite materials used

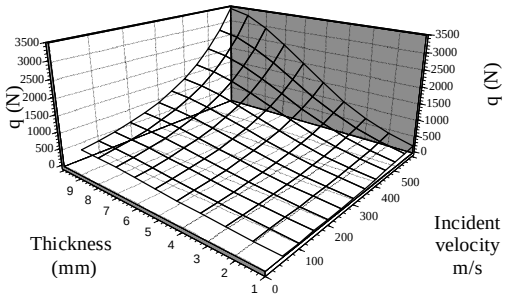

Figure (6) 3-D force thickness velocity for Plain 2.5*2.5 E-Glass epoxy.

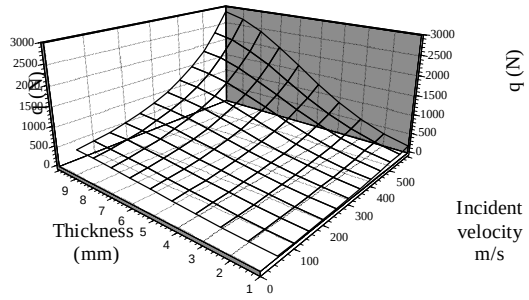

Figure (7) 3-D force thickness velocity for Plain 2.5*2.5 E-Glass Polyester

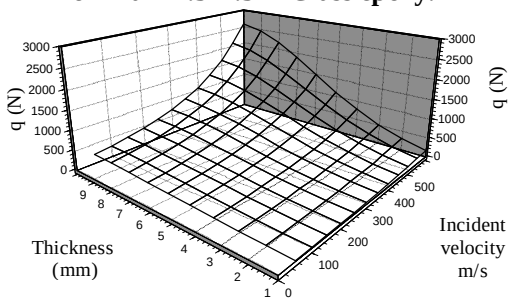

Figure (8) 3-D force thickness velocity for Plain 12.5*12.5 E-Glass Polyester

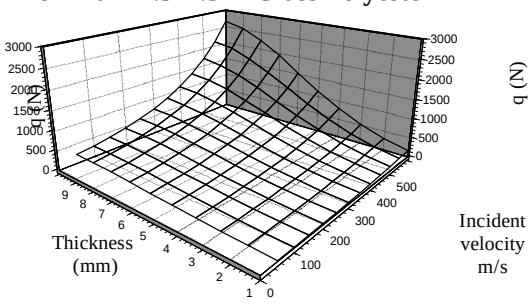

Figure (9) 3-D force thickness velocity for 5-end satin 5*5 E-Glass Polyester

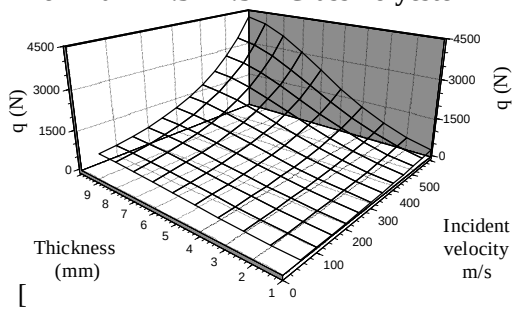

[

Figure (10) 3-D force thickness velocity for Random E-Glass Polyester

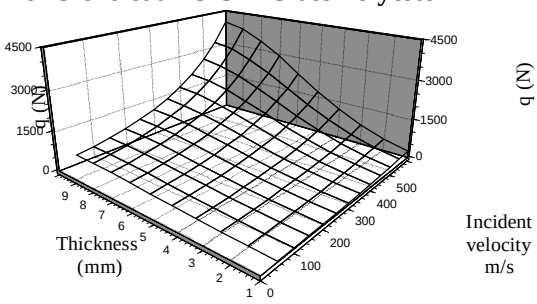

Figure (11) 3-D force thickness velocity for Plain 7*7 Carbon Polyester

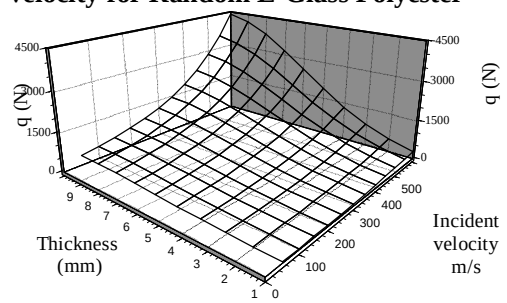

Figure (12) 3-D force thickness velocity for 5-end Satin 5*5 Carbon Polyester.

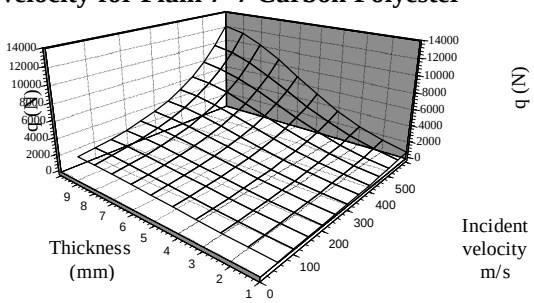

Figure (13) 3-D force thickness velocity for 3-end Satin Kevlar Polyester.

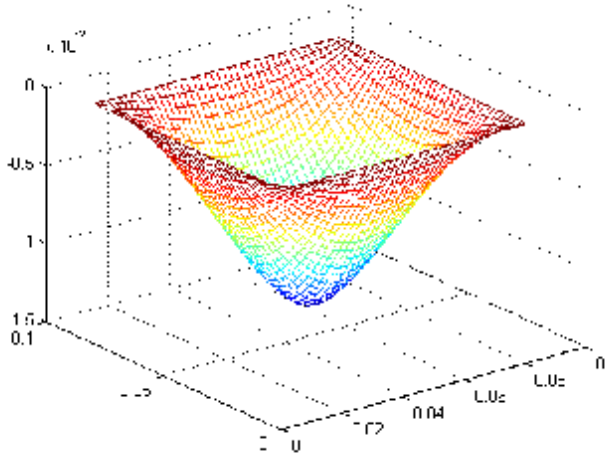

Figure (14) Maximum elastic deformation of clamped two layers 3-end satin fiber reinforced polyester plate (80*80mm) impacted by 7.5g rigid impactor with V_i=100m/s and r_p=1mm.

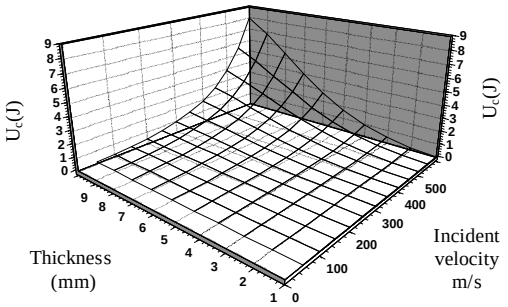

Figure (15) 3-D Contact energy (Uc)~ thickness- velocity for Plain 2.5*2.5 E-Glass epoxy.

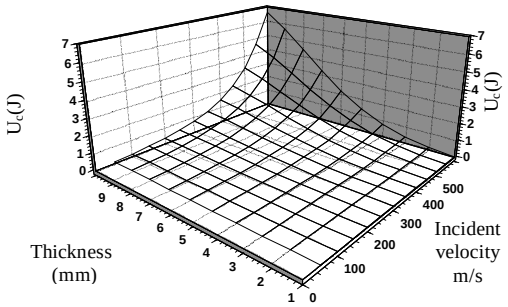

Figure (16) 3-D Contact energy (Uc)~ thickness- velocity for Plain 2.5*2.5 E-Glass Polyester.

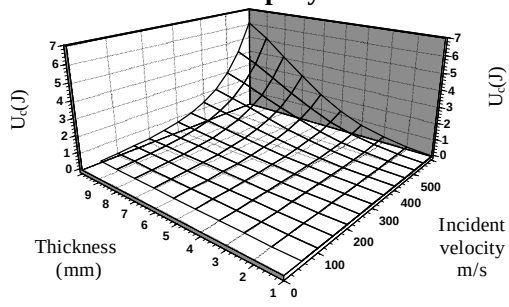

Figure (17) 3-D Contact energy (Uc)~ thickness- velocity for Plain 12.5*12.5 E-

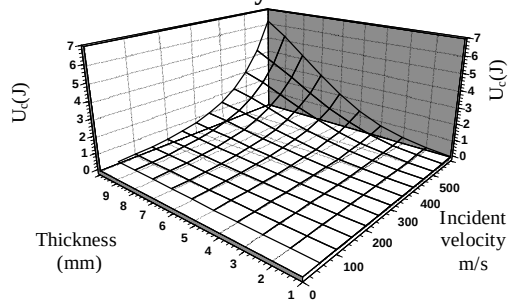

Figure (18) 3-D Contact energy (Uc)~ thickness- velocity for 5-end satin 5*5 E-Glass

Glass Polyester.

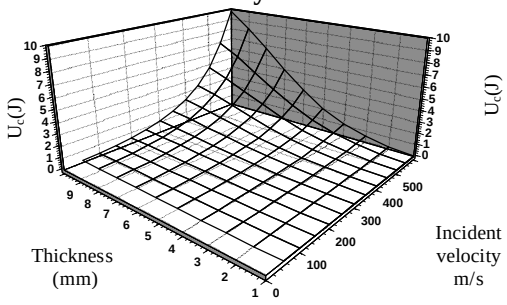

Figure (19) 3-D Contact energy (U_c)~ thickness- velocity for Random E-Glass Polyester.

Polyester.

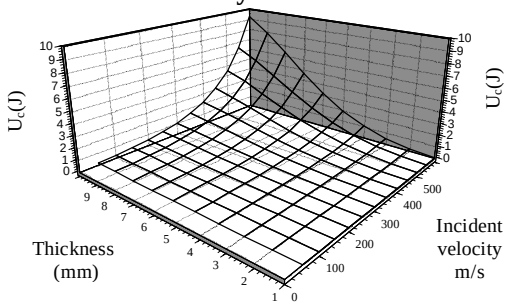

Figure (20) 3-D Contact energy (U_c)~ thickness- velocity for Plain 7*7 Carbon Polyester.

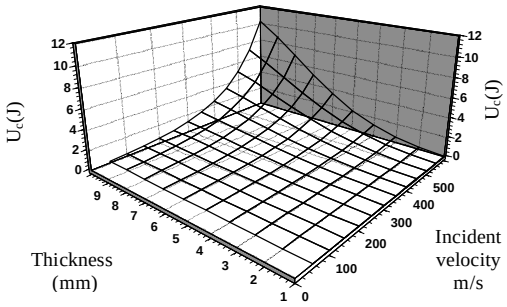

Figure (21) 3-D Contact energy (U_c)~ thickness- velocity for 5-end Satin 5*5 Carbon Polyester.

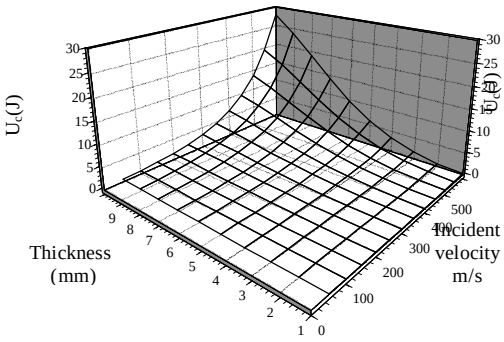

Figure (22) 3-D Contact energy (U_c)~ thickness- velocity for 3-end Satin Kevlar Polyester.

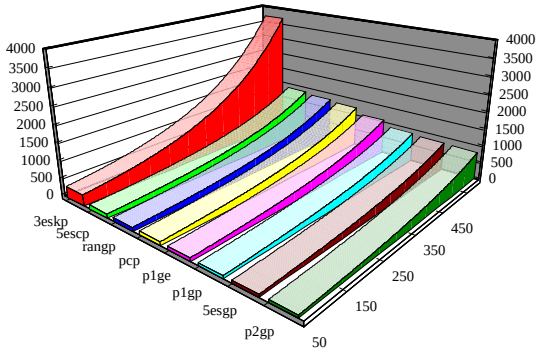

Figure (23) contact force for materials used for plate with 4mm thickness for different incident velocities

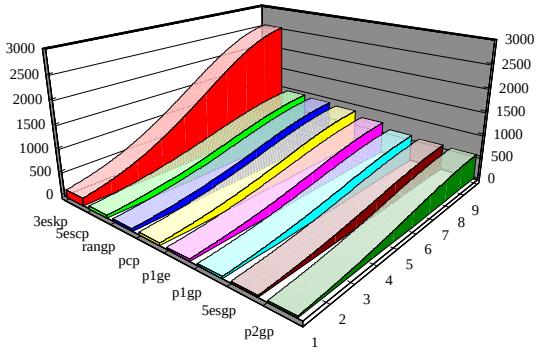

Figure (24) contact force for materials used for plate for different thickness with 250m/s incident velocities.

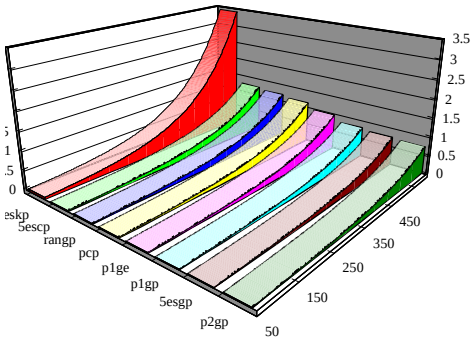

Figure (25) contact energy for materials used for plate with 4mm thickness for different incident velocities.

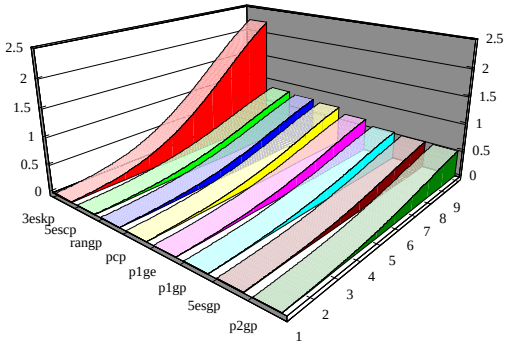

Figure (26) contact energy for materials used for plate for different thickness with 250m/s incident velocities.

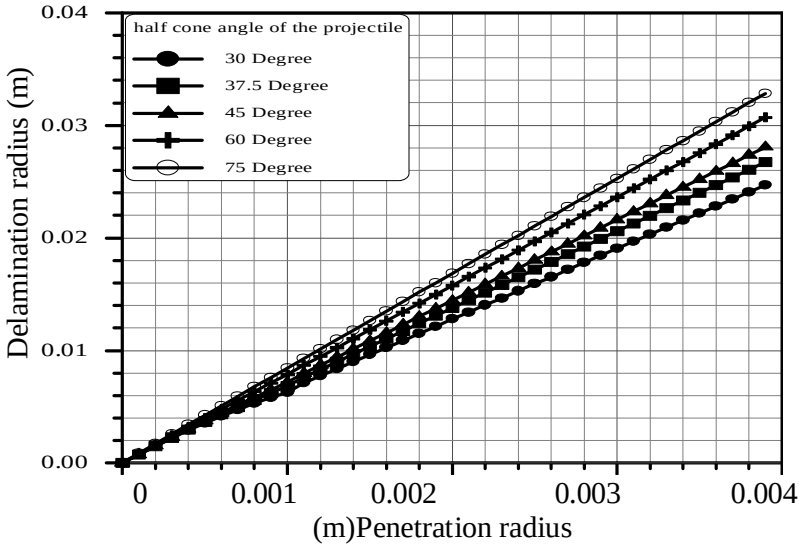

Figure (27) Delaminating radius versus local projectile radius.

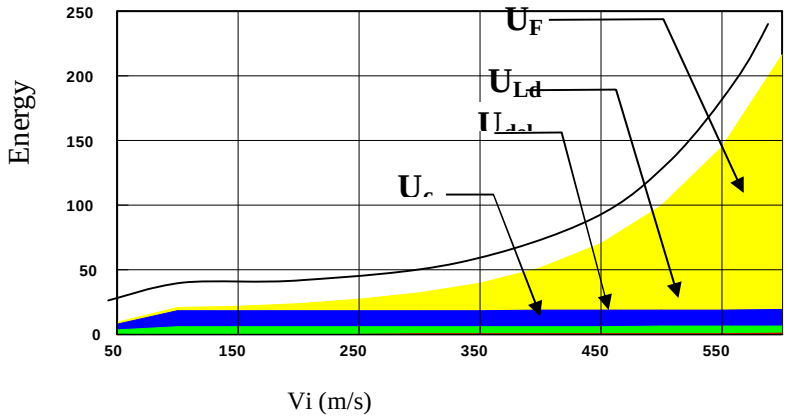

Figure (28) The absorbing energies duo to impacting 60° cone angle 7.5g rigid projectile to a (80*80) mm2 Plain-woven 2.5*2.5 E-Glass reinforced polyester for 4mm thickness

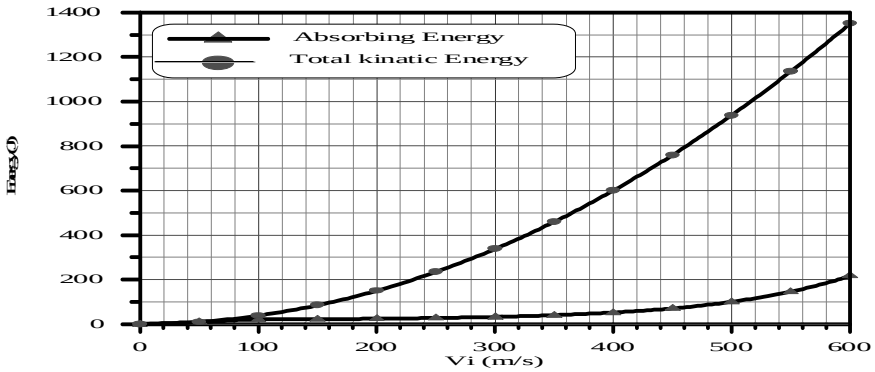

Figure (29) The total Kinetic Energy of the projectile and the absorbing energy versus the impact velocity.

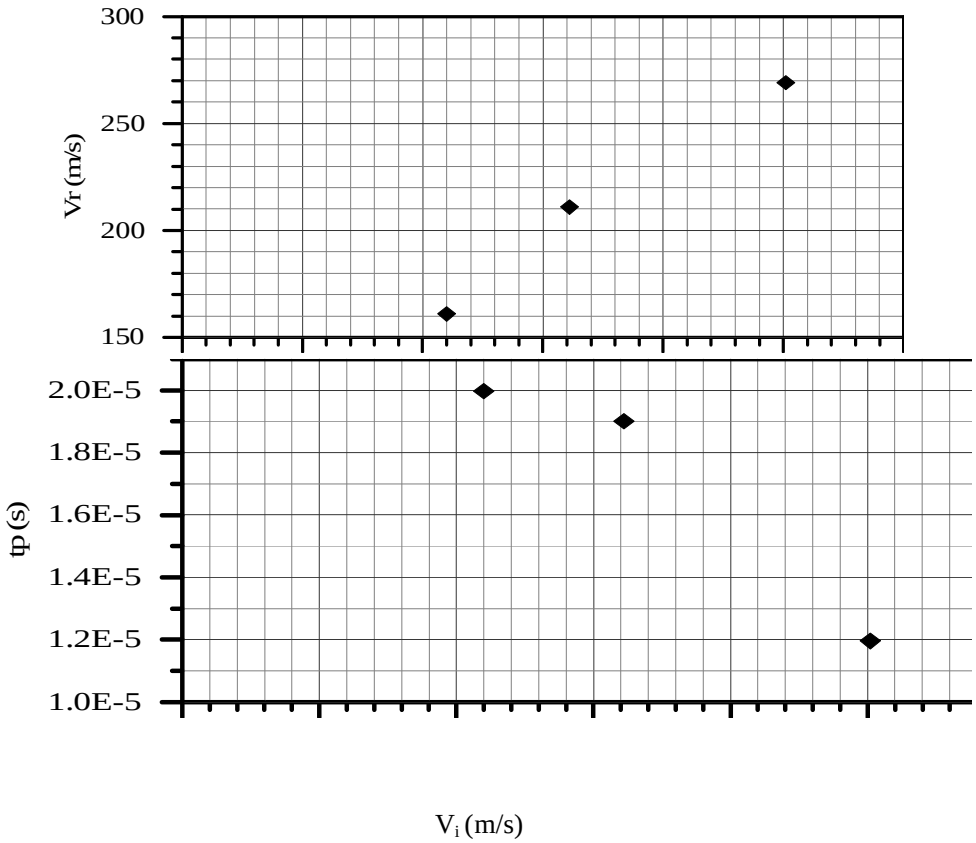

Figure (30) The Impact experimental results of the 10-layers p1gp (h=3.9mm), impacted by 60°, 7.5 g steel projectile for various incident velocities